FIZIKA Volume 21, Supplement 1, 1989.
Proceedings of the XI Yugoslav SYMPOSIUM OF THE PHYSICS OF CONDENSED MATTER.
M. Davidović and M. Lj. Napijalo Editors, Donji Milanovac, October 3–7, 1988.

BEAM-INDUCED MODIFICATION OF CRYSTALLINE SOLIDS

Tomislav M. Nenadović
The Boris Kidrič Institute of Nuclear Sciences, P.O.B. 522, 11001 Belgrade, Yugoslavia

In this review some aspects of beam-induced modification of solids at atomic and microscopic scale are presented. The beam interaction with solids is or may be relevant for fundamental effect of interaction processes, changes of solid properties, as well as useful tool for study of the behaviour of solids. As in all cases the changes start at solid surfaces, a special attention has been drawn to them.

1. Introduction

Interaction of particle and electromagnetic radiation, with solids add to a variety of physical and chemical phenomena. Changes, induced in crystalline solids, where the atoms are regularly arranged, depend on beam characteristics and target properties.[1] The physical phenomena of solid crystal modification, induced during beam or working fluid interaction include: radiation damage effects in crystal producing vacancies, interstitials (Frenkel pairs) and their clusters;[2] structural changes in which the incident beam in the range of atomic collisions cascade in crystal produce amorphization and recrystallization;[3,4] compositional changes in the case of non elemental targets as a result of variation in sputtering (erosion) yield of the components;[5] topographical changes with different surface features due to erosional and redepositional phenomena;[6,7] other desirable and nondesirable effects on the material exposed to the beam.

Whatever if the mechanism of beam-induced modification of material properties, if the bombarded doses are high enough, the modification of solid surfaces is observed. The observed surface relief formed on the material exposed to the beam or working fluid is usually of different types: blisters and gas bubbles - from inert gas ions implanted in the metal; grain relief with cliff at the grain boundaries - on polycrystalline target as a result of orientation dependence of sputtering; facets with shape dependent or orientation - on single crystals; cones or pyramids in localized regions of different sputtering rate - due to dirt, inclusions or, erosional and redepositional processes at different surface localities.[8]

In this paper the results of beam-induced modification of crystalline solids, by different type of incident beams (particles and electromagnetic) are presented.

While the range of incident beam in solids is short (medium energy) the deposition of energy tends to be accumulated at the surface layer. As a consequence, the bombardment leads to bombardment-induced morphological changes of surface: in this experiment by collisional (physical) sputtering, laser sputtering and mechanical sputtering (erosion) of elemental and alloy target.

2. The basic concept of beam-induced modification

The irradiation of a crystal leads to degradation of the material properties. Usually metal lattices show a high degree of perfection on an atomic level. For all crystallographic structures crystal is built of an infinite regular array of atoms, arranged on a space lattice of perfect periodicity.[9] When an energetic beam strikes on the ordered crystal, a small localized disordered region can be produced.[10] The incident beam particles scattered several times on target atoms, creates a primary recoil atoms which in turn collide on other regular array of atoms and collision cascade develops.[11] The minimum energy to displace an atom from its lattice site (threshold energy Ed) is of the order of 25 eV. If some of the primary displaced atoms (secondary, etc) obtained sufficient energy to overcome the surface binding, various spacies will be ejected; the bombarded surface is sputtered and many effects on atomic, microscopic and macroscopic scales can be observed.[12]

Any type of incident beam may be used in studies of the interaction phenomena with solids. The relatively limited irradiation conditions for introducing defects in a controlled manner were made possible in nuclear reactors. Later it was found convenient to use a wide range of well controlled sources of beam irradiations. In the beam experiments, the beam parameters such as: mass (M), energy (E), dose (D) and incident angle (θ) are well controlled, so that more information on interaction mechanisms could be obtained.[13,14] The most commonly used incident beams are:

- charged particle beams (protons, deuterens, inert gas ions, fission fragments and electrons), and
- uncharged particle beams (neutrons, γ-ray and laser beam).

The probability of a lattice atom to leave the lattice side depends on the specific parameters of crystal: structure, chemical composition, defect concentration and temperature. The quantities which are of the greatest interest for the analylis are:

- number of collisions (N_s) between the incident radiations and atoms of the solid,

$$N_s(cm^3/sec) = n\ v\ N\ \sigma$$

(n - density of the incident particles, v - velocity, N - atomic density of solids σ - cross-section of the particular event).

the distance travelled in the solid (R-total range) before coming to rest - range of radiations,

$$R = 0.6 \frac{Z_1^{2/3} + Z_2^{2/3}}{Z_1 Z_2} \cdot \frac{M_1 + M_2}{M_1} M_2 E$$

(index 1 for incident beam, 2 for target)

-distribution of defect structures along the path of radiation through the solid (isolated Frenkel pairs and displacement cascades).

The sharp threshold model is widely used in calculations of atomic displacement in crystalline solids, but it is not quite realistic. Besides, it should be pointed that the charge state of the moving particle (in metals) is of minor importance.

From the point of view of solids (based on the point defects formed $N_F = E_c/E_d$, where E_c is the primary recoil energy), the most interesting effects are:

- production of impurities, by implantation of incident particles (example, Ar^+) or by transmutation of lattice atom ($^{70}Ge+n \rightarrow {}^{71}Ge \rightarrow {}^{71}Ga$)

- production of high energy particles (in nuclear fission in ^{235}U, $E_{h.f.} = 67$ MeV and $E_{h.f.} = 95$ MeV; or nuclear reactions, $^6Li(n,\alpha)^3H$ with $E = 2{,}1$ MeV),

- heating of the target to the relatively high temperature (transient effect) in certain regions of the solid ($Ar \xrightarrow{+50\ keV} U$, $T \simeq 400^oC$; $h\nu$ (laser or δ) $\rightarrow$ M)

- excitation of the electrons which is not an important effect in metals (it is more important in bio-materials, polymers, organic crystals etc.).

Beam induced modification of materials for scientific and applied interest occurs over a wide range of energies, from keV to about 100 MeV. The incident particles may range from electron, through hydrogen and heavy ion to the regular or irregular species (dust particles). It is quite impossible to make a review of all possible combinations of radiation, energy interaction mechanisms (elastic or inelastic collisions) and modification of material properties.[15] Generally, along the path of the radiation in solids; electron beam altered mechanical properties, neutron beam - electrical and magnetic properties, ion beam - thermal and surface properties as well as chemical reactivity, finally uncharged beam, because of local heating, has the greatest influence on diffusion processes in solids.[16] But if the range of different radiation presented in table 1 is analysed - one can conclude that it is in all cases short. Hence, the changes are most expressed on the surface and beam induced morphological changes are mutual for all combinations of incident beams and target materials. For this reason a greater part of the paper is dedicated to these changes and illustrated with results of the experiments performed in the author's laboratory.

Table 1. Range of some radiations in solids

Beam	E	R
Ar^+	10 keV	5 μm
	50 keV	25 μm
Xe^+	10 keV	1,3 μm
	50 keV	6,8 μm
D^+	2 MeV	10 μm
Kr (fission f)	95 MeV	6 μm
Xe (fission f)	67 MeV	"
e	MeV	0,1 cm
n^o	MeV	2 cm
γ	1 MeV	3 cm
LSR	$4x10^3 J/cm^2$	0,08 μm
	$4x10^4 J/cm^2$	0,95 μm

3. Experimental

The experimental method used in these investigations includes bombardment of flat and cylindrical surfaces with different type of incident beam.

The ion bombardment was performed in the collector region of an electromagnetic isotope separator.[17] This experimental arrangement gives well defined parameters as ion species, energy and incident angle of the beam. The ion beam density was between 20-150 μA cm^{-2} for flat target and 40-200 μA cm^{-2} for cylindrical target depending on the beam energy; it was held constant during each experiment. The residual gas pressure in the collector region during bombardment, $5x10^{-7}$ torr or better. The neutron bombardment (n_{th}) was performed in nuclear reactor.

The laser sputtering was examined on thin films and coatings, previously prepared by sputtering deposition in vacuum. The energy density of the beam was focused to a spot of a radius of 200 μm. The pulse duration was 15 μs.

As target material for the investigation of surface changes during the working cycle, the rotating (free standing) blades of medium pressure 300 MW gas turbine have been used. Parts of a new blade have been placed into quasi real conditions (MP-LP cylinder connecting tube). The used turbine blades - for erosion examination - are randomly selected (by visual inspection).

The beam induced modification was investigated using optical microscope, carbon replicas (TEM) and scanning electron microscope (SEM). The composition of selected regions could be determined by electron microprobe (EPMA).

4. Results and discussion

4.1. Gas bubbles and blisters

The first effect of surface modification observed during ion sputtering, at the dose of 10^{17} ions/cm^2 was surface blistering. Blisters are formed on the surface of a target during ion bombardment, when conditions for a high gas concentration near the projected range of implanted inert gas ions are suitable. The presence of gas bubbles was firstly observed during neutron irradiation of fission materials.[18] The first analysis of the gas bubbles formation and blistering for implanted ions was performed by implanted He ions in copper.[19] Now this

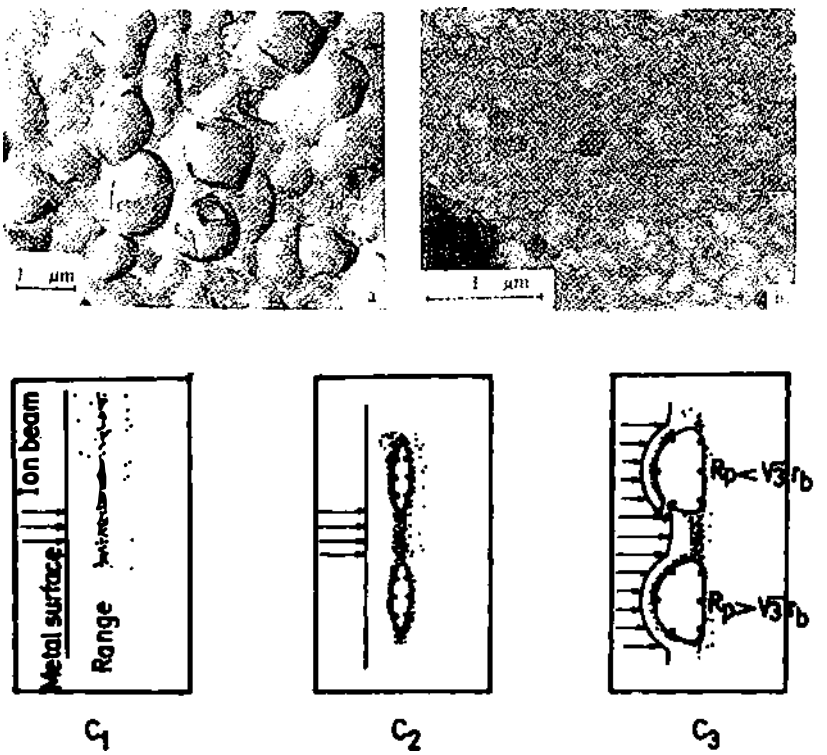

Fig.1.(a-c) Blistering on bombarded uranium: a - replica showing blisters on surface after bombardment with He ions up to dose of 10^{17} ions/cm^2; b - transmission electron microscopy of gas bubbles; and c - stages in blisters formation.

problem is a serious limitation for many aspects on the inner wall of fusion reactor technology.[20)]

In our experiments blistering has been firstly observed during He bombardment of U, at the dose of 5×10^{16} by means of one stage carbon replicas. The blisters form as a result of coalescence of small bubbles which occur when the solubilities of implanted gas in the bombarded target is small.[21)] The coalescence of two bubbles at the constant volume results in an excess internal pressure in the larger bubble, because of the fall in the balancing surface tension term ($p = 2\gamma/r$). The possible mechanism of blisters formation is shown on Fig.1.(a-c): gas implantation in the range distribution, atoms and vacancies combination to form small bubbles, critical density for small bubbles coalescence (forming large flat volumes of high pressure gas) and gas bubbles expansion up to plastic deformation of the overlaying implanted zone. It was found that the critical pressure of the gas ($p_c > 10^3 kg/cm^2$) in the small bubbles of diameter r_b which results in blisters is given by

$$p_c = \frac{Y}{1 + ctg^2\theta_m} .$$

where: Y is the yield strength of the material and θ_m the angle between the surface normal and the direction of crack propagation. The maximum stress for crack formation

$$\max = \frac{R_p^2 + r_b^2}{R_p^2 - r_b^2}$$

It should be pointed out that better results for the behaviour of inert gases in solids are obtained from direct observation of inert gas bubbles by means of the transmission electron microscope (Fig.2a). Some elements (isotopes of, $^{6}_{3}Li$, $^{9}_{4}Be$, $^{10}_{6}B$ and $^{235}_{92}U$) which transmute under neutron bombardment produce the inert

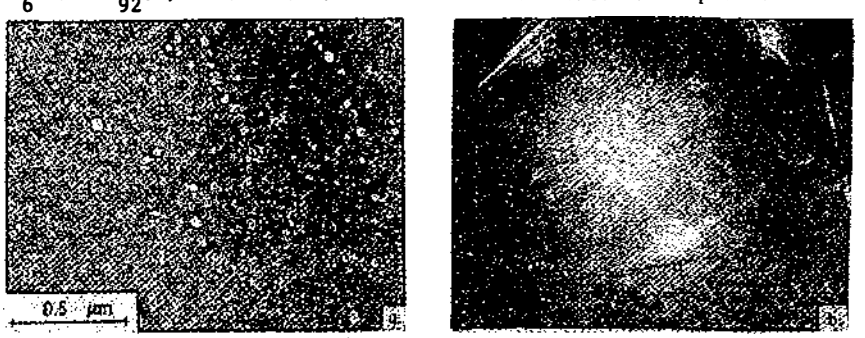

Fig.2.(a and b) Aluminium film containing: a - small helium bubbles after AlLi bombardment with 10^{20} n/cm^2 (annealed 2h at 300°C); and b - Kikuchi lines in a diffraction pattern of thick film (Ar^+ ions, E=40 keV and d=10^{16}ions/cm^2)

gas atoms as products. In our experiment for example we used the Al-Li (1%) alloy (2a). The inert gas atoms He are produced by nuclear reaction $_3Li^6(n,\alpha)_1H^3$ But when the thickness of a sample is increased, Kikuchi lines are formed (2b) as a result of the inelastic scattering of electrons. The Kikuchi lines are the evidence for a high degree of crystalline perfection.

Using the perfect gas law equation, the pressure and number of gas atoms in a bubble can be related to bubble radius.[22]

$$p = \frac{2\gamma}{r}, \qquad pV = nkT, \qquad V = \frac{4}{3} r^3 \pi$$

$$n = \frac{8\pi\gamma r^3}{3kT}$$

Direct observation of bubbles (in TEM) has shown that they migrate through the solid by a diffusion process.[23] The bubble diffusion coefficient (D_b) can be expressed by means of surface diffusion coefficient (D_s) or volume diffusion coefficient (D_v). The migration velocities (v) is given by

$$v = \frac{1}{8\pi} \cdot \frac{D_s}{kT} \cdot \left(\frac{a_o}{r}\right)^4 \cdot F$$

where: a_o - is the lattice parameter (for fcc crystal) and F is the driving force which produces bubble motion.

Although the bubbles behaviour as well as the radiation damage in solids are a complex many-body problem, usually they have been treated only by making drastic approximations.[24] In many experimental conditions region of high local damage is more important than in the case of two-body collisions between beam particles and stationary atoms of solids.[25] Such, a more complete feature of modification in solids is given in models: dynamic stages of radiation damage and fission damage in metals.

4.2. Ion beam sputtering topography

The elementary features on the bombarded surfaces arise from different sputtering of individual crystal grains, different erosion rate in small local regions and surface imperfection. The sputtering theories based on a momentum transfer between the incident ions and target atoms, as well as the earliest attempt where the ions dissipate sufficient energy in a small region so that target atoms can evaporate, did not predict sputtering topography phenomena.

According to the theory the sputtering yield generally depend on the projectile energy (E), penetration depth (R_p) and angle of incidence (θ), as well as on target properties (surface binding energy U_o, M_2 and Z_2)[13]

$$S(E,R_p,\theta) = \frac{042\ f(E,\ R_p,\ \theta)}{N\ U_o(\mathring{A})^2}$$

where $f(E, R_p, \theta)$ is the deposited-energy depth distribution.

From the experiments it is deduced that the sputtering yield is dependent on the possible energy transfer in the first collision and the mean free path of the ion (λ) into the bombarded target:[26)]

$$S = K \frac{1}{\lambda(E)} \cdot \frac{M_1 M_2}{(M_1 + M_2)^2} \cdot E$$

The evolution of surface features during ion bombardment was not adequately explained by considering only the variation of sputtering yield with the ion incident angle, or local surface contaminat processes (dirt, inclusion, other atoms etc.). These results are obtained on the basis of the earliest systematic studies on spherical targets. Secondary effects, as redeposition of sputtered particles, surface enhanced diffusion of adsorbed atoms and species and radiation damage effects, play an important role in sputter-topographic evaluation of surfaces. Experimental results enabled important number of theoretical models.[27)] Consequently the collisional theories and atomic displacement predict that the cone shape depends only weakly on the ion beam energy.[28)]

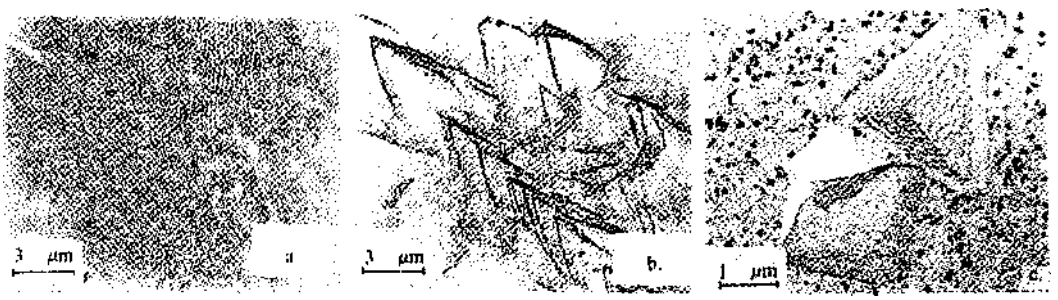

Fig.3.(a-c) Surface modification of a polycrystalline target bombarded by 40 keV argon ions (one-stage carbon replica): a - aluminum with $7 \cdot 10^{16}$ ions/cm^2; b - platinum with $6 \cdot 10^{18}$ ions/cm^2 and c - uranium with $8 \cdot 10^{18}$ ions/cm^2.

Our earliest studies of sputtering topography by replicas have shown, that various forms of bombarded features can be obtained.[29)] Modification of the initial surface during ion bombardment give three groups of surface features: furrowed structure, wave structure and cone like structure presented on Fig.3.(a-c). All features are dose dependent (10^{16} - 10^{19} ions/cm^2) and we suggest that the crystallographic variation of sputtering is the main reason of the surface topography.

The angle of incidence variation on appearance on pyramids or cones was studied by amorphous, dielectric and polycrystalline fibres bombardment from one direction, normal to the fibre axis; all those angles of incidence (from 0^{o} to 90^{o}) are represented. Under conditions when $S=S(\theta)$ the sputtering is not uniform over the surface; thus the contour changes from circular to the conical form (Fig.4.) The cross-sectional profile of cylindrical fibres bombarded by Ar^{+} ions, energy of 3-18 keV (4a) is observed in all bombarded amorphous targets; pyrex, lead-glass, silica-glass and capillar (diameter up to 130 μm). But at certain energies (2 keV, 16 keV) the topography includes ledge on the base of the cone, not predicted by theoretical works (4b). The study of cross section profiles of metal wires was of interest just for the investigation of the charge accumulation that may result in ion deflection and step formation.[30] During bombardment, all metal wires were grounded, so the possibility of charging effects and ion deflection were elliminated. In spite of this, the ledge formation were also observed (4c). It was evident that the charge accumulation did not contribute to the mechanism of ledge formation. Because of the crystalline characteristics the wires profile and contour evolution could not be measured accurately.[31] Clear evidence of cone, or pyramide generation was found on upper surface of bombarded wires. The cone axis is in the direction of the beam incidence, the apex angle and the mean cone height decrease with increasing ion energy. Hence, the variation of cone characteristics are similar with the variation of resulting geometry obtained on amorphous fibers.

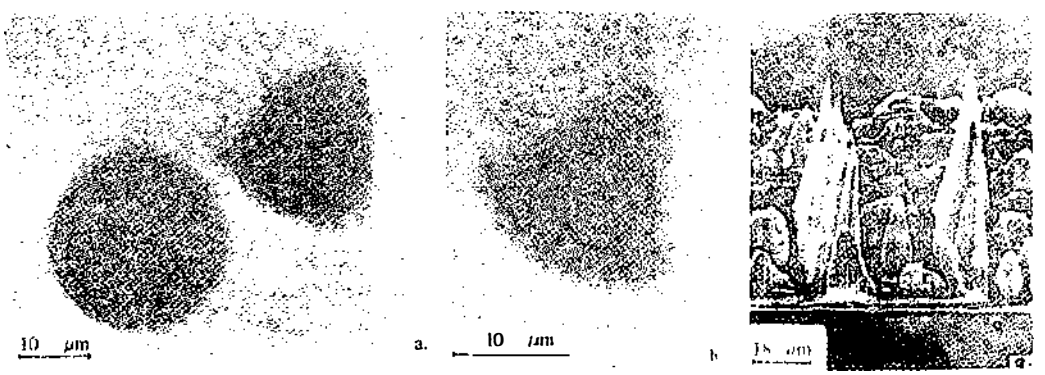

Fig.4.(a-c) Cross-sectional profile and contour of a sputtered fibres:
a - unsputtered and sputtered silica (Ar^{+} ions, 6 keV, 10^{17} ions/cm^{2});
b - quartz (50 keV, 10^{19} ions/cm^{2}) and c - gold (50 keV, 10^{19} ions/cm^{2}).

A carefully controlled experimental investigation of cylindrical geometry did not get satisfactory results concerning angular dependence of sputtering yield. For the energy of 9 keV and higher the $S(\theta)$ curve is quite reasonable and

in agreement with the results obtained by other method. Maximum sputtering yield θ_{max} is at about 75^{o}, and the critical angle for total reflection θ_{cr} is decreasing sharply nearly to zero. But for the energy of 6 keV and lower the peak profile is moved towards lower values and does not include the high expected characteristics Disagreement of the angular dependence of sputtering yields and surface topography were at the highest for the alloyed wires. On the basis of the obtained results it was possible to conclude only, that two-component alloyed wires showed preferential sputtering and that the microstructure of non-elemental target played an important role during topography development.

Therefore, we thought that measurements of these quantities on flat target of binary alloys would be of particular interest. As a target we have chosen: binary alloy which form solid solutions with relatively simple phase diagrams (Fe-Ni and Fe-Cr) as well as two-phase system which in whole concentration range of the components is an eutectic composition (Ag-Cu).

The mean sputtering yield of the binary alloy can be calculated according to the definition, as a number of sputtered atoms/ number of incident ions. We determined the total sputtering coefficient (S_t) of the alloy on the basis of the following expression:[32)]

$$S_t = S_1 c_1 + S_2 c_2 ,$$

where: S_1 and S_2 are the sputtering coefficients of the component in the alloy, and c_1 and c_2 their concentration in the target.

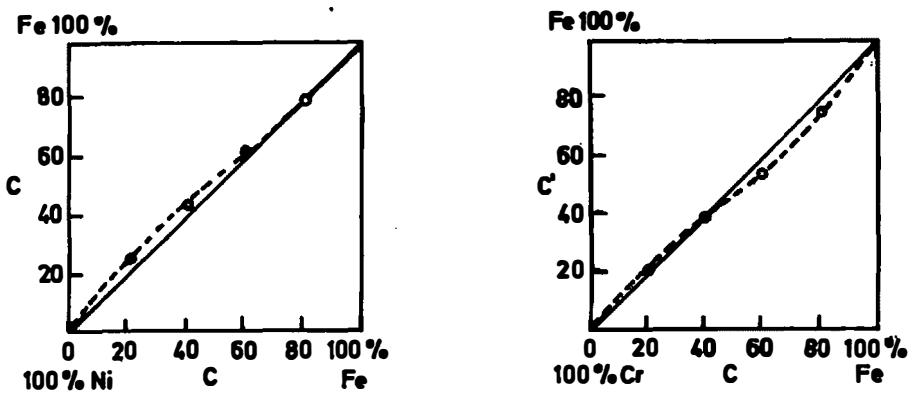

Fig.5.(a and b) Chemical composition of sputtered deposit as a function of the compositions of the bombarded alloys; a - FeNi and b - FeCr (Kr ions, E=4 keV and d = $4 \cdot 10^{17}$ ions/cm^2).

The experiment revealed that the composition of sputtered deposits (collected on glass and aluminium and determined by means of AAS and EPMA) differs from those

of the target. On Fig.5.(a and b) the results of compositional changes of sputtered deposits as a function of target material composition are presented. One can see: 1. - the sputtering coefficients of the elements in alloys are different from the same values of pure component; 2. - at high Ni concentration (Fe-Ni alloy) the sputtered material contains 4-5% more Fe than the target; 3. - with high Fe concentration (Fe-Cr alloy) the deposited material contains Cr to a similar extent. Such a result is a consequence of small bombardment doses ($4 \cdot 10^{17}$ ions/cm^2). Theoretically, if the bombardment dose is high enough, the composition of sputtered deposit must be the same as the composition of the bombarded target. From the same reason the developed surface structure has shown intensive etching effect presented on Fig.6.(a-c). Only for bombarded Fe-Cr the surface had hardly expressed topographical features (in case of Fe-Cr the dose was higher for factor 2 than for other targets).

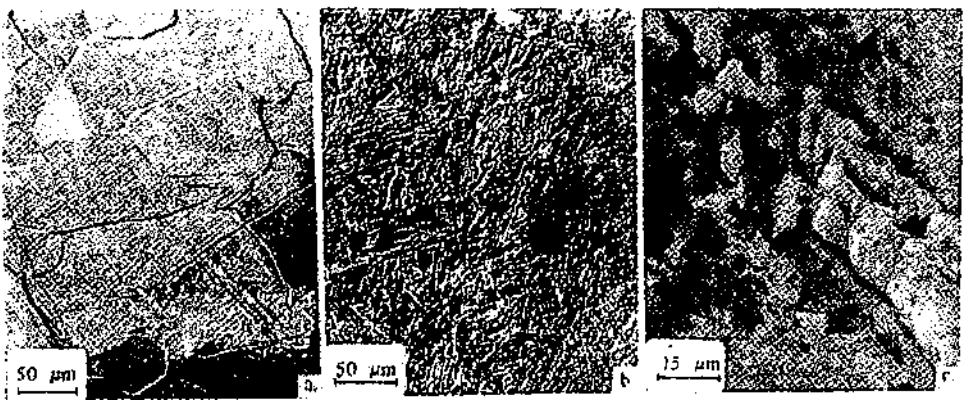

Fig.6.(a-c) Ion beam etching of: a - pure Fe, b - FeNi (80:20) and c - FeCr (60:40). (Kr ions, E=4 keV and d=$3 \cdot 10^{17}$ ions/cm^2)

The Ag-Cu alloy was bombarded up to the higher dose (10^{19} ions/cm^2). The results (Fig.7.) have shown that the sputtering yield of the alloy is defined by the product of the sputtering yields of pure components and the ratio of their concentration.[33] Although for small ion doses it is expected that the sputtering yield should have higher Ag concentration comparing to the initial alloy composition (as in previous experiments) for high doses the steady-state contition is reached. Then Ag and Cu are sputtered in the same ratio in which they are in the bombarded target. Consequently, the relative sputtering rate of Cu from the alloy is much higher than that from pure metal (the opposite is for Ag).

The observed topography of AgCu after bombardment with Ar^+ ions to a dose of 10^{17} ions/cm^2 has shown: 1. - island region formed from Cu grains (~90% Cu) with a small concentration of Ag; 2. - textured matrix formed from eutectic

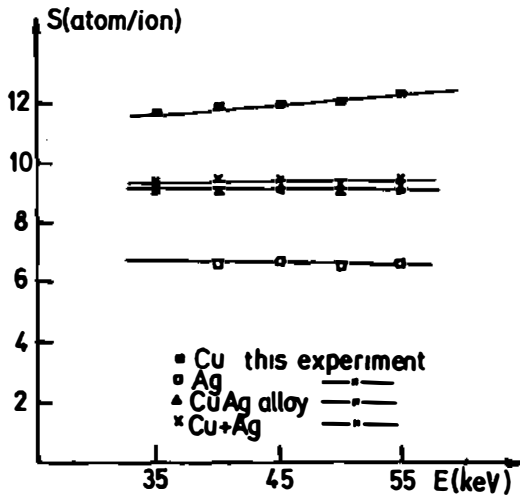

Fig.7. Sputtering yields for Ar^+ ions on Cu, Ag and CuAg alloy.

mixture of Ag($\sim$ 60%) and Cu crystallites, arises from the relative higher sputtering rate of silver crystallites.[34] With increasing dose - to 10^{18} ions/cm^2 - the microstructure revealed by preferential sputtering (of Ag in eutectic mixture) changed as a result of angular dependence of sputtering. The sharp ridges were formed. Finally, at the highest bombardment dose - 10^{19} ions/cm^2 - in the same region a dense concentration of cones was formed due to copper islands formation on the bombarded surface (by surface diffusion and redeposition) and preferential sputtering of silver. For all doses, the observed topography depends on the copper crystallites orientation.

The variation in topography between two regions of different preferred orientations is illustrated on Fig.8.(a-c). The difference arises from the fact that the formation and aggregation of defects - to form clusters - is strongly orientation dependent (8a). The preferential sputtering in the vicinity of clusters formed during ion bombardment and angle of maximum sputtering yield for different crystal orientations represent probably the first stadium of cone formation. Due to the channeling effect of the beam, the erosion rate is also orientation dependent. The variation of topographical features with ion energy is in agreement with previous measurements. In the region of a mixture of small Ag-Cu crystallites, the cone profile and height are found to change with ion energy (8b). Further, in the copper region we have observed cones formed by two different mechanisms: 1. - in the edge pits, the cones are formed by redeposition

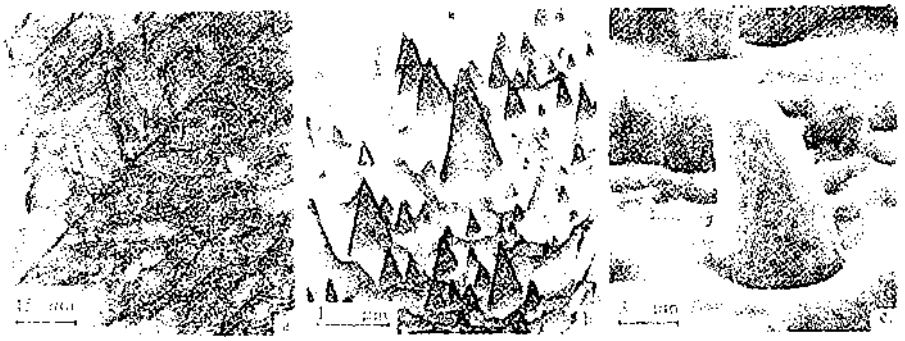

Fig.8.(a-c) The variation in surface topography: a - as a function of orientation of copper crystallites (E=55 keV, d=10^{19} ions/cm^2); the density of cones is higher in the upper left-side region, where the copper grains are heavily faceted; b - distribution of cones profile and height; c - deformed cone in faceted etch pits.

of sputtered materials - as a result of plastic deformation they are often deformed (8c); 2. - the large individual cones (randomly distributed) are formed below masking particles left on the surface as a result of shadowing the copper surface.

4.3. Sputter deposition of thin films and coatings

Sputtering is the process in which material is ejected from a solid by a momentum transfer process. Only a part of the incident beam energy (1%) is used

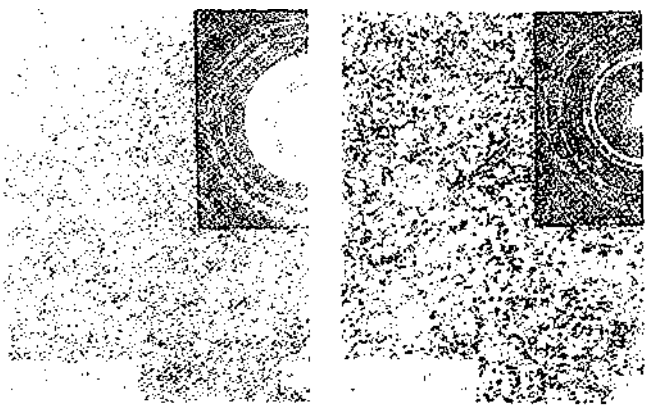

Fig.9.(a and b) Transmission electron micrograph of thin films (Au onto glass) deposited at room temperature; a - ba vacuum evaporation and b - by ion beam sputtering.

to produce sputtered particles (about 75% is used for heating the target, and rest is associated with the emission of secondary electrons).[35] If any substrate is placed on the path of sputtered atoms on the surface, thin film or coating (depending on the thickness) will form.[36,37] A wide variety of coating methods are available.[38]

A bried advantage of sputtering deposition is the following:

- Sputtered thin films or coatings have different grain size than evaporated (Fig.9.(a and b))
- Sputtered deposits of the same material adhere more strongly to the surface.
- The sputtered deposits contain considerable amounts of gas (which can be avoided during evaporation at low pressure).
- The impurities on the surface can have a strong influence on nucleation and growth of thin films.[39]

4.4. Laser beam sputtering

Laser beam (or photon) sputtering and modification of surfaces is not a momentum-transfering process. On time-scale, for the various types of sputtering, laser sputtering is for factor 10^2-10^4 sec slower comparing with collisional processes.[40] Such a process is attributed to sputtering by vaporization from the surface of the transiently heated impact region. Other processes which can occur are: ion sputtering (manifested by the appearance of plasma near the target surface and characteristic conical topography) and exfoliational sputtering (induced by

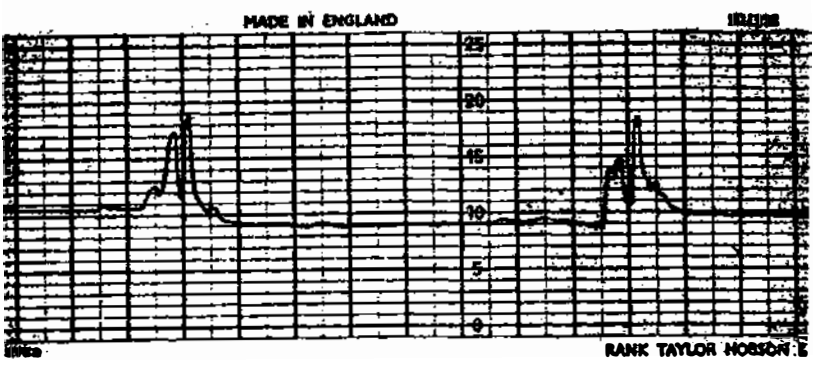

Fig.10. The profile of the laser irradiated region, with three zones of modification (crater, steep swell and gentle roughness).

thermal stress cracking and blistering). In order to analyse the mechanism of the process, the maximum surface temperature reached during each pulse should be known (value is difficult to deduce, because the efficiency of energy deposition and loss is not available). If this temperature is high enough the crater of the thermal sputtering will be formed.[41] The thermal sputtering coefficient (S_{th}) is obtained by equating the rate of vaporization with the rate of condensation as well as the equilibrium vapor was present.

$$S_{th} = \int\int p(2\pi mkT)^{-1/2} \cdot 2\pi y \, dy \, dt \text{ (atoms/ion)}$$

where p is the vapor pressure of target material, m is their mass, k is the Boltzmann's constant and t=f(y,t) is the known function of the energy deposited by an incident ion in a single cascade.[8]

The laser sputtering yield of Ti thin films (deposited by rf sputtering) is determined from the material losses during the interaction and the obtained profile.[42] Typical shape of the irradiated region - obtained by profilometric

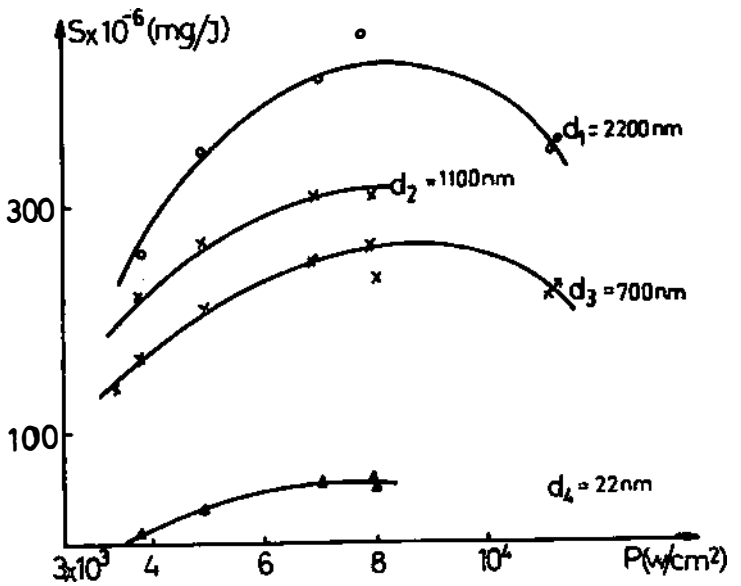

Fig.11. The laser sputtering yield of Ti coatings as a function of the beam densities for different film thicknesses.

measurements (Fig.10) - show three zones. They are: well shaped crater in the central part (evaporation and ejection of material), steep swell at the hole edge and the zone of slightly expressed roughness.[43] The craters profile is energy dependent: their width and depth increase with increasing the laser power densities (YAG:Nd). Consequently, sputtering yield increased with increasing beam energy and the film thicknesses.

The results of sputtering yield as a function of laser beam densities are presented on Fig.11. It can be seen, that the sputtering yield has a maximum at the laser beam densities of about 8×10^4 W/cm^2. Decreasing of sputtering yield at higher power densities is a consequence of the target screening with plasma.

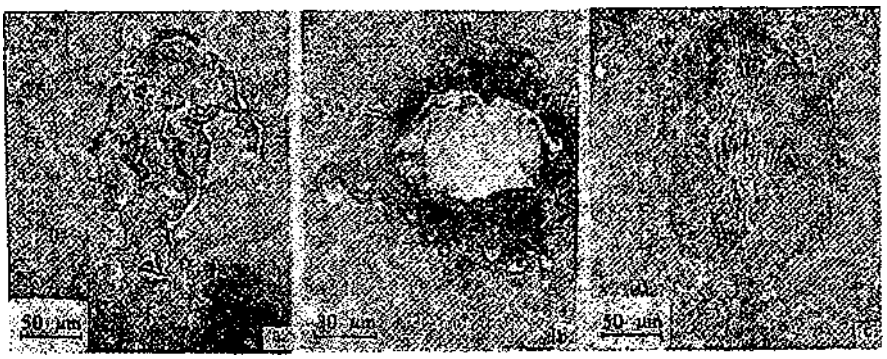

Fig.12.(a-c) Scanning electron micrograph of laser irradiated region:
a - exfoliation and thermal stress cracking, b - non-uniform melting and ejection of droplets, and c - topography of melting with the swell around the crater.

More detailed studies of the irradiated region by scanning electron microscopy have shown that different mechanisms of sputtering have occured.[44] For all energies, the shape of the bombarded region is almost circular (Fig.12). A part of the beam energy is absorbed and the other part is reflected. At low energy ($\sim 1 \times 10^3$ W/cm^2) the surface did not melt uniformly: it exfoliated and showed topography remaining solid (mostly) with thermal stress cracking effect (12a). For medium energy, the surface topography showed non-uniform melt characteristics of the crater. In the area around the spot thickness changes occur, and the crater is surrounded with ejected droplets of different diameter (12b). For the highest energy, surface topography of the crater is indicative of melting (thermal sputtering). A liquid metal solidifies quickly on the edge of the crater and the step swell is formed (12c).

4.5. Mechanical sputtering

Solid surfaces exposed to ion beams, working fluids, or hard oxides particles and species may become modified. In real devices (steam turbine, fusion devices, spacecrafts) different mechanisms of surface degradation play an important role. One of them, mechanical sputtering (removal or etching) shows unexpected similarities with some aspects of ion and laser beam material modification.[45] Up to now results have shown that the data are available only in a narrow zone mass-velocity.[46]

In our experiment the investigation of mechanical sputtering during beam interaction has been performed on the constructing stainless steel (material of medium pressure turbine blades). The results of erosion damage are shown on micrographs in Fig.13.(a-c). Morphological changes in the damaged zone have shown that

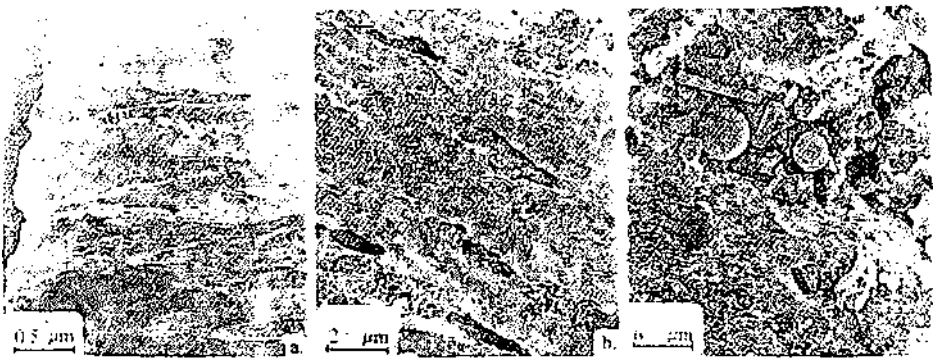

Fig.13.(a-c) Mechanical sputtering of structural stainless steel;
a - at glancing angle, b - individual impact damage and
c - fast moisture droplets interaction.

the mechanism of erosion is mechanical sputtering (13a). Individual collisions with beam particles (dust) occured at glancing angles and the energy transfered during interaction is dissipated within the surface area. Depth of damage in this zone is small. Two other mechanisms during interaction, are observed also. The first are craters formed during the interaction with irregular oxide species (13b). It was found empirically that the crater volumes (V_{cr}) are nearly linear function of the impact energy:[47]

$$V_{cr} = a_{cr}\, m_p\, v_p^2$$

where: m_p - particle mass, v_p - impact velocity and a_{cr} - travelled distance.

The crater diameter (if we neglect the dependence of crater form and volume on the densities of projectile and target) is found

$$d_{cr} = m_p^{1/3}\, v^{2/3}$$

(where d_{cr} is in cm, m_p in gr and v in km sec^{-1}). Finally, the last type of damage is a large area with erosion spot obtained during interaction with spheroidized fast moisture droplets containing: oxygen, salts and oxide particles (13c). The initial damage is liquid impingement erosion.

It is interesting to point out, according to experiments, that the angular dependence of the mechanical sputtering is the same as in case of physical sputtering.[48]

Acknowledgements

This work is performed by author and coworkers of the Atomic Physics Institute, IBK-Vinča. The parts of the experimental work were supported by SKNE (Yugoslavia), CEA (France) and USA (NBS) - Yugoslavia Joint Board Project. Author would like to express his gratitude to all of them.

References

1) G.M.McCracken and P.A.Scott, Nuclear Fusion 19,N°7(1979)889
2) W.D.Wilson, M.I.Baskes and C.L.Bisson, Phys.Rev. B13(1976)2470
3) E.C.Baranova, V.M.Gusev and I.B.Haibullin, Rad.Effects 18(1973)21
4) H.M.Naguib and R.Kelly, J.Nucl.Mat. 35(1970)293
5) J.W.Candern, J.Vac.Sci.Tech. 17(1980)72
6) G.K.Wehner and D.J.Hajicek, J.Appl.Phys. 42(1971)1145
7) A.D.Stewart and M.W.Thompson, J.Mat.Sci. 4(1969)56
8) O.Ausiello and R.Kelly Ed. Ion Bombardment Modification of Surfaces, Elsevier, Amsterdam, 1984
9) J.Friedel, Ann.Phys., t.I, N°6(1976)257
10) M.W.Thompson, Defects and Radiation Damage in Metals, Cambridge, U.P., 1969
11) R.Kelly, Rad.Effects 80(1984)273
12) S.K.Lam and M.Kaminsky, J.Mat.Sci. 89(1980)205
13) P.Sigmund in Sputtering by Ion Bombardment (Topics in Appl.Physics, Ed. by R.Berisch) Springer, 1980
H.H.Andersen and H.L.Bay, ibid, 1981
14) H.Oechsner, Appl.Phys. 8(1975)185
15) K.L.Merkle in Physics of Ionized Gases, Proc. SPIG, Rovinj, 1974
16) J.Cousty, R.Peix and B.Perraillon, Surf.Sci. 107(1981)586
17) I.Ševarac, B.Perović, B.Dunjić and R.Protić, Nucl.Instr. 3(1958)245
18) A.T.Churchmann, R.S.Barnes and A.H.Cottrell, J.Nucl.Mat. 7(1958)88
19) R.S.Barnes, G.B.Redding and A.H.Cottrell, Phil.Mag. 3(1958)25

20) S.L.Das, M.Kaminsky and R.Tishles, J.Nucl.Mat. 85/86(1979)225
21) G.M.McCracken, Rep.Prog.Phys. 38(1975)241
22) R.S.Barnes and D.J.Mazey, Proc.Roy.Soc., A275(1963)47
23) R.S.Barnes, J.Nucl.Mat. 11,2(1964)135
24) V.Levy and M.Gerl, J.Microscopie 4, N°5(1965)594
25) Y.Quere, Ann.Phys. 5(1970)105
26) F.A.Kol, J.Flut and J.Kistemaker, Physica 26(1960)1009
27) G.Carter, J.S.Colligon and M.J.Nobes, J.Mat.Sci. 6(1971)115
28) P.Sigmund, J.Mat.Sci. 8(1973)1545
29) T.Nenadović, Z.Rundić and T.Dimitrijević, Bull. B.Kidrič Inst.Nucl.Sci. 20, Vol.2(1969)9
30) B.Meckel, T.Nenadović, B.Perović and V.Vlahov, J.Mat.Sci. 10(1975)1188
31) T.Nenadović, N.Bibić, B.Meckel and M.Milosavljević, Nucl.Inst.Meth. 182/183(1981)319
32) M.Riedel, T.Nenadović and B.Perović, Acta Hem.Ac.Sci.Hungaricae 97(1978)177
33) N.Bibić, T.Nenadović and B.Perović, Proc. 7th IVC, Vienna 1977, p.1485
34) N.Bibić, I.H.Wilson and T.Nenadović, J.Appl.Phys. 53, N°7(1982)5250
35) L.Maissel and R.Glang, Handbook of Thin Film Technology, Mc Graw Hill, New York, 1970
36) T. Nenadović, Z.Fotirić, T.Dimitrijević and M.Adamov, Thin Solid Films 10(1972)45
37) M.Adamov, B.Perović and T.Nenadović, Thin Solid Films, 24(1974)89
38) K.L.Chopra, Thin Film Phenomena, Mc Graw Hill, New York, 1969
39) R.Gupta and B.Perraillon, Surface Sci. 103(1981)397
40) R.Kelly and J.Rothenberg, Nucl.Inst.Meth. B7/8(1985)755
41) R.Kelly, Rad.Effects 80(1984)273
42) T.Mihać and T.Nenadović, Proc.Phys.Ion.Gases, Inst. of Physics, Belgrade, 1984
43) K.Yoshii, M.Umeno, S.Murata, H.Kawabe, K.Yamada, I.Watanabe and T.Kubo, J.Appl.Phys. 55,1(1984)223
44) T.Mihać and T.Nenadović, Proc.Phys.Ion.Gases, Univ. of Sarajevo, Sarajevo, 1988
45) T.Nenadović, N.Popović and J.Fine, J.Mat.Sci. 24(1989)3699 s
46) J.Kissel and F. Krueger, Appl.Phys. A42(1987)69
47) F.Hortz et all, Planet.Space Sci. 23(1975)151
48) T.Nenadović, B.Perović and R.Simović, Bilten JUVAK 23(1989)99